

Zone of flow establishment in turbulent jets

Dimitriadis P., Liveri-Dalaveri M., Kaldis A., Kotsalos C., Papacharalampous G. and Papanicolaou P.
 Department of Water Resources and Environmental Engineering, National Technical University of Athens
 (www.itia.ntua.gr)

1. Abstract

It is well established experimentally that as the Reynolds number increases the core of the jet diminishes and has smaller effects on the jet's mean profiles (e.g. concentration, temperature, velocity). The scope of this project is to examine this relationship based on dimensional analysis and experimental data. For that, spatio-temporal concentration records are obtained on the plane of symmetry of heated vertical round jets (for a laboratory turbulent scale at the order of mm) using tracer concentration measurements via a planar laser induced fluorescence technique (PLIF). The investigation area is set close to the nozzle of the jets (up to 10 jet diameters away), at the zone of flow establishment (ZFE), so as to determine the geometric characteristics (dimensions and shape) of the core as a function of the initial velocity and nozzle diameter. The ZFE is estimated through the absence of turbulent intensity fluctuations (assuming a threshold value of 1% of the maximum intensity).

2. Introduction

The jets are widely used in several engineering fields mainly for wastewater/salt disposal, gaseous releases etc. Using engineering terms, investigation of the zone of flow establishment (ZFE) "seems both futile and unnecessary in view of its limited extent" (Jirka, 2004). Nevertheless, in scientific terms, it is of high importance as it includes the shear layer and transition to turbulence. The ZFE is defined as the area within the shear layer developed at the edge of a jet and is known to have a 'conical' shape, because of the shear layer dispersion towards the jet axis at the advancing of the jet (Chen & Nikitopoulos, 1979). The limit of that dispersion is the axis of symmetry and its distance from the nozzle is considered as the ZFE length (x_c), which is affected by flow instability and thus it is difficult to define. It is generally observed that as the Reynolds number increases, distance x_c decreases. A literature survey is done along with some measurements of x_c in time and space via PLIF visualization to verify this view. Specifically, three locations are recorded that are based on the time-averaged (TAV) and root-mean-squared (RMS) images of rhodamine 6G concentration C. The first at the point where the TAV of C at the jet-axis starts to decay ($x_{c,m}$), the second where the RMS of C takes values above a threshold ($x_{c,sm}$), and the third where the normalized RMS of C ($x_{c,smax}$) is maximum.

3a. Literature survey (experimental values)

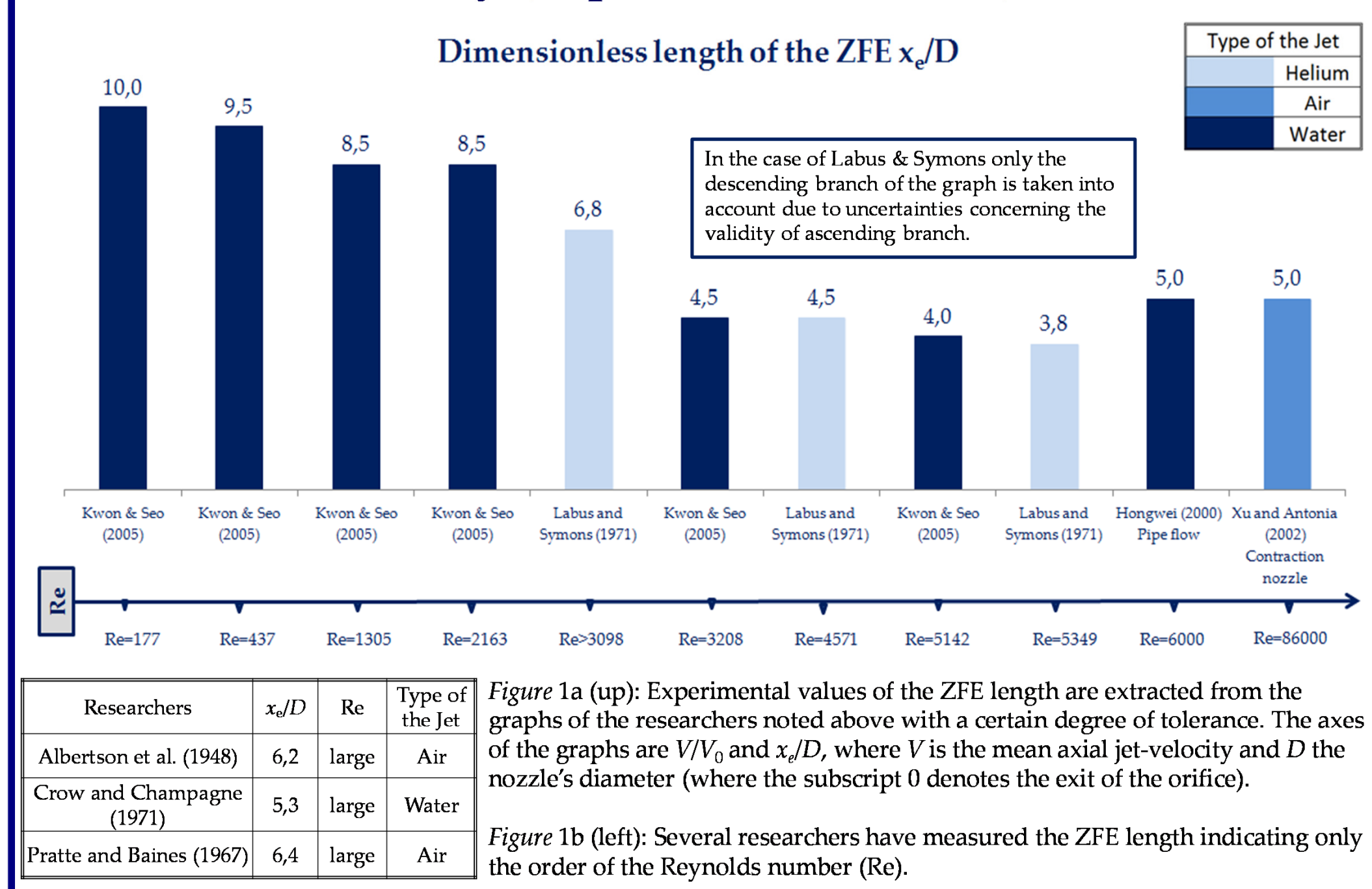


Figure 1a (up): Experimental values of the ZFE length are extracted from the graphs of the researchers noted above with a certain degree of tolerance. The axes of the graphs are V/u_a and x_c/D , where V is the mean axial jet-velocity and D the nozzle's diameter (where the subscript 0 denotes the exit of the orifice).
 Figure 1b (left): Several researchers have measured the ZFE length indicating only the order of the Reynolds number (Re).

3c. Literature survey (approximated equations)

Lee & Jirka (1981) have given a solution of X_c as a function of F_0 for a stagnant uniform waterbody of large horizontal extent. X_c increases rapidly from zero for $F_0 \rightarrow 0$, to an asymptotic value of 5.74 for F_0 greater than 25. This is somewhat smaller than the value of 6.2 determined by Anderson et al. (1950).

$$1 + \frac{4}{F_0^2} \left(\frac{X_c}{12} + \frac{\sqrt{\pi} \lambda \epsilon}{12} X_c^2 + \frac{\lambda^2 \epsilon^2}{3} X_c^3 \right) = \frac{(1 + \lambda^2)^2}{8 \lambda^4 \epsilon^2} \frac{1}{X_c^2}, \text{ where}$$

$$X_c = x_c / D, \text{ the ZFE length normalized around the diameter}$$

$$\epsilon = 0.109, \text{ jet spreading angle}$$

$$\lambda = 1.14, \text{ ratio of temperature diffusion thickness to momentum diffusion thickness}$$

According to Jirka (2004) the ZFE length is measured from a linear spread of the shear layer and estimated about $6.2 D$, based on velocity profiles, or about $5 D$, based on scalar profiles, due to the typical dispersion ratio, $\lambda > 1$. This fundamental result is generalized for cross-flow effects using the empirical approach of Schatzmann (1978), and for buoyancy effects through model formulation by Lee & Jirka (1981). They suggest

$$x_c = 5D \left(1 - 3.22 \frac{\sin \gamma_0}{V/u_a} \right) (1 - e^{-2.0 F_0 / 4.67}), \text{ where } \gamma_0 = \sin^{-1} \left(\sqrt{1 - \cos^2 \theta_0 \sin^2 \sigma_0} \right) \text{ with}$$

σ_0 , the angle measured counterclockwise from the ambient current direction

to the plane projection of the orifice centerline and

θ_0 , the angle between the orifice centerline and the horizontal plane.

$$\text{Note that for } u_a = 0: x_c = 5D (1 - e^{-2.0 F_0 / 4.67})$$

4. Experimental set-up

An experiment using planar laser-induced fluorescence (PLIF) visualization is set at the laboratory of Applied Hydraulics of the NTUA in order to determine the geometric characteristics (intrusion length and shape) of the core. The experiment is set-up as follows:

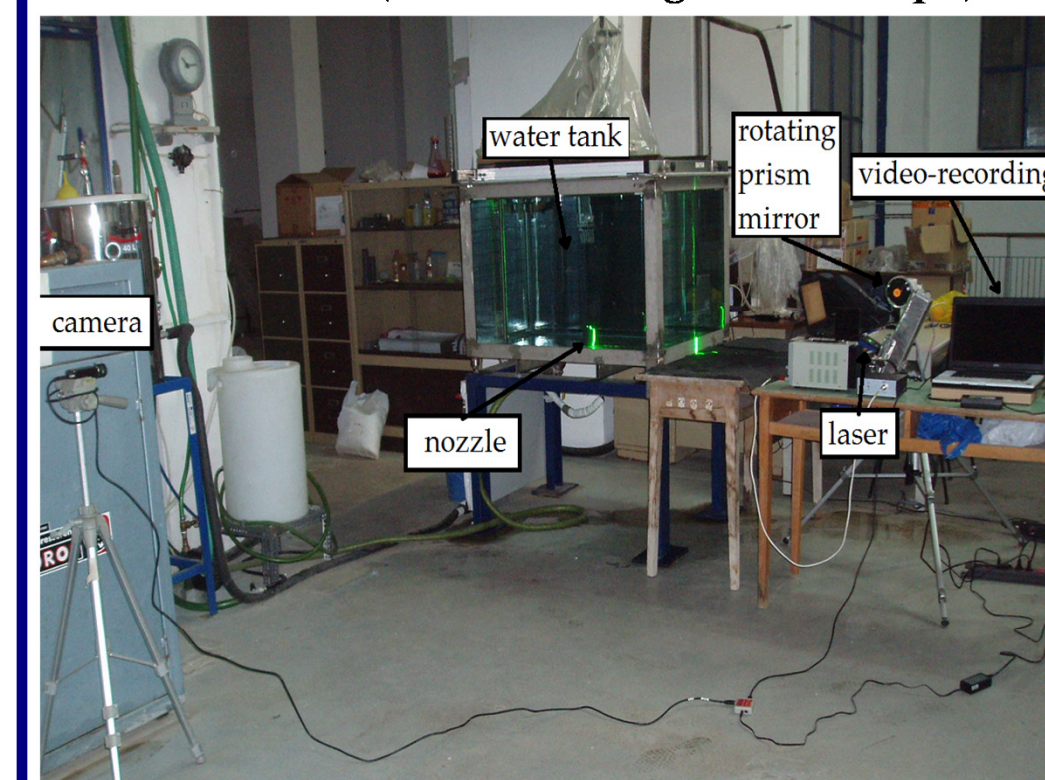


Figure 2: PLIF experimental set-up (NTUA, Laboratory of Hydraulics)

- A jet is heated (buoyant) and dyed with a rhodamine 6G (R6G) substance and then exits from a nozzle of diameter D to ambient water of lower temperature.
- A DPSS 1 W laser beam at 532 nm wavelength (green), is converted to a thin laser light sheet via a rotating prism mirror (at 20 kHz). R6G emits 556 nm light (yellow) when excited by the 532 nm light making visualization possible.
- A high resolution video-camera is then used to videotape the flow field. In this manner, the light intensity of R6G (measured through the RGB 8bit frame format of the camera) can be converted to concentration.

The camera is set at the plane of symmetry of the jet, at a distance of at least $0.75 \times D$ meters from the nozzle, so as to achieve a window-view height greater than 10 diameters. The width of the window is chosen to be at least 3 diameters long to capture the jet expansion (at an angle of 12° - 15° with respect to jet axis). Each video lasts around 25 sec, and is recorded at 12 frames per second (fps), so as to achieve stationarity.

5. Calibration

The initial fluorescence light intensity I_0 can be assumed to be proportional to the R6G initial concentration C_0 for values less than $50 \mu\text{g/l}$ (Ferrier et al., 1993). A decrease in power and light intensity occurs as the laser beam enters the water tank and travels through the dyed jet. For this range of concentrations and over a small path length (of order of 1 cm), the power attenuation can be assumed to be negligible (Walker, 1987). Thus, only the light intensity attenuation factor is taken into account and the raw data are modified according to Walker (1987) formula:

$$I(x) = I_0 e^{-\sum \eta_i x}, \text{ with } \eta_i = \eta_w + \epsilon_i C, \text{ where}$$

x_i is the distance the laser beam travels through water (from pixel $i-1$ to i),

η_w and ϵ_i are the laser beam attenuation coefficients through water and R6G, respectively.

Measurements within an adequate range ($1-60 \mu\text{g/l}$) of concentration intensities (fully mixed into the water tank) are made in order to determine the attenuation coefficients ϵ_i and η_w (as shown in figure 3).

The red intensity of the RGB color format and a shutter speed (SS) of 50 msec are chosen as the optima, based on image resolution and data quality criteria.

The image scale Sc and lens' distortion (pixel size variation along height) are estimated from a ruler placed on the nozzle. The average value of Sc is considered as it only varies $\approx 2\%$.

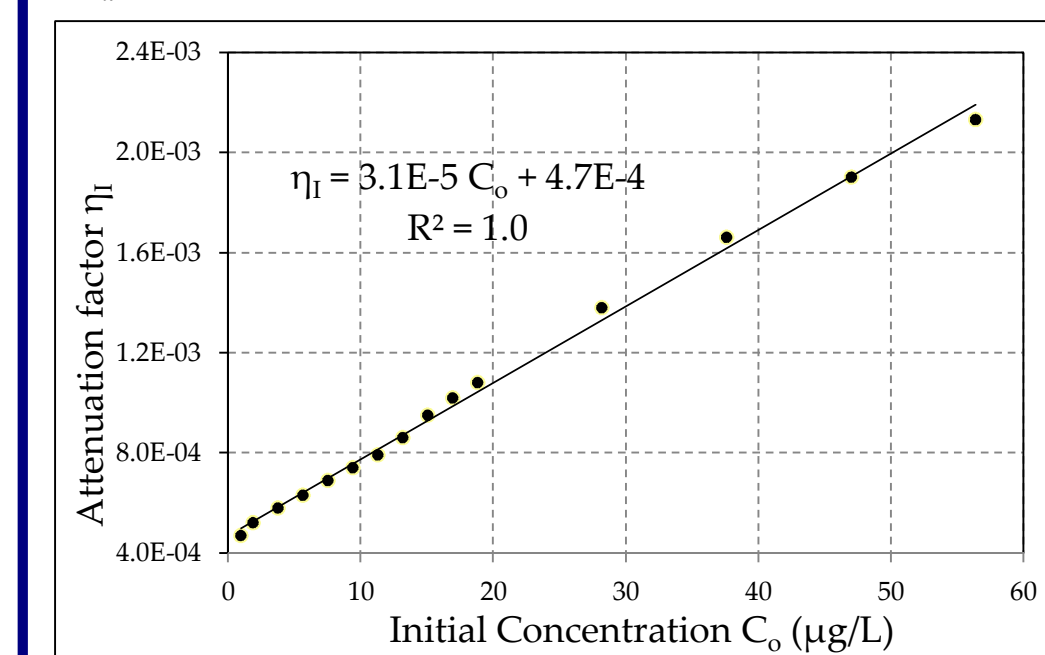


Figure 3: Light intensity attenuation factor, where ϵ_i is the slope ($3.1 \cdot 10^{-5}$) and η_w the intercept ($4.7 \cdot 10^{-4}$) of the trendline.

6. Data processing

Four jet diameters are tested (0.5, 1, 1.5 and 2 cm) for a range of initial discharges (Q) 5 to 40 cm^3/s ($\pm 0.85 \text{ cm}^3/\text{s}$) with Reynolds numbers $\text{Re} = 10^2$ - 10^4 and Froude numbers $F_0 = 1$ - 200 .

Flow instabilities occurring within the ZFE may result in a non axisymmetric jet:

a) Noise from the camera (estimated via recording with the camera lens covered), background noise (estimated via recording with no jet discharge) and noise from slow motion of ambient water (observed from suspended particles) is estimated to be less than 1% (fig. 6).

b) A fountain-like periodic movement of the core is observed within the ZFE.

The length and shape of the core are estimated through the absence of turbulent intensity fluctuations rather than the presence of a constant initial jet concentration. This is achieved by the standard deviation image rather than the mean or the instantaneous one. Image and data processing are done using MATLAB®.

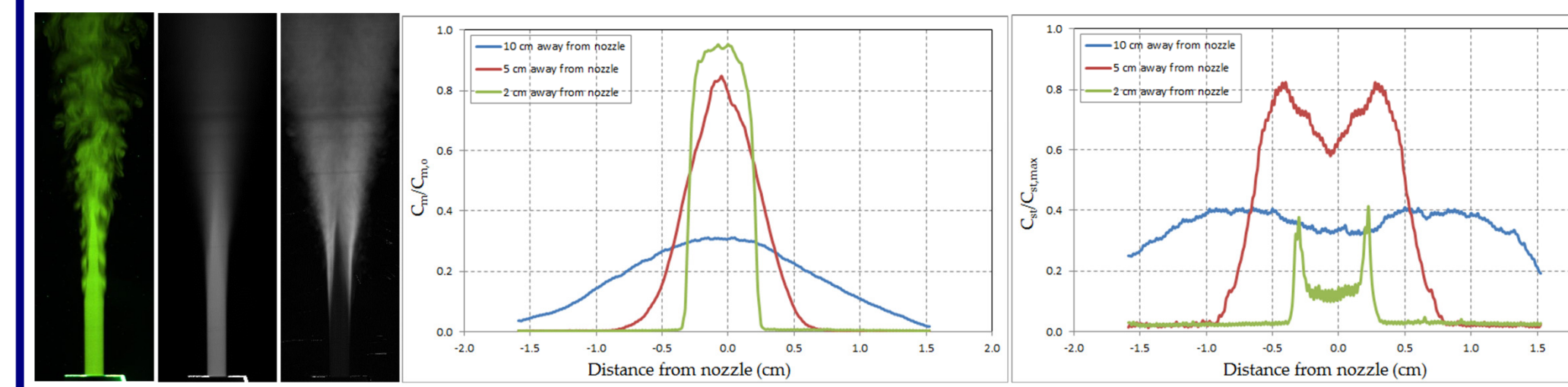


Figure 4: Instantaneous, time-averaged and RMS images (green and gray images, left). Normalized mean and standard deviation distributions with their maximum values (middle and right figure, respectively) at a distance of 2 cm (within the ZFE), 5 cm (around the end of ZFE) and 10 cm (outside the ZFE) from the nozzle.

7. Experiments performed

Here, the initial conditions of the conducted experiments as well as the measured x_c are presented.

Symbol memo	Exp1	No	1	2	3	4	5	6	7	8	9	10	11	12	13	14	15	16	17	18	19	20	
D (cm)	0.5	Frames	360	244	508	510	521	511	509	510	507	508	473	449	515	621	459	508					
Sc (cm/px)	0.0225	Q (ml/s)	5.2	6.0	6.9	8.6	10.2	11.9	13.6	15.3	16.9	18.6	20.3	22.0	23.6	25.3	27.0	28.7	30.3	32.0	33.7	35.4	
SS (msec)	50	Re	1418	1646	1875	2331	2788	3244	3700	4157	4613	5070	5526	5983	6439	6896	7352	7809	8265	8721	9178	9634	
Fr (fr/sec)	12.0	Fr	28.5	33.1	37.7	46.8	56.0	65.2	74.4	83.5	92.7	101.9	111.2	120.4	129.6	138.8	148.0	157.2	166.4	175.6	184.8	194.0	
Tamb (°C)	23.3	Tamb (°C)	4.60	2.20	1.86	1.16	1.16	1.36	1.26	1.0 ^a		0.86	0.96	0.96	0.9 ^a	0.9 ^a	1.16	1.56					
Tamb (°C)	14.1	x _{c,m} (cm)	6.26	4.26	3.16	2.76	2.46	2.16	2.0	1.96	1.66	1.4 ^a	1.26	1.1 ^a	1.16	1.16	1.76	1.76	1.76				
Tamb (°C)	1.732	x _{c,sm} (cm)	8.76	5.56	3.96	3.76	3.36	3.0	2.96	2.4 ^a		3.96	2.56	2.56	2.6 ^a	2.6 ^a	3.16	2.56					
Tamb (°C)	2.312	x _{c,smax} (cm)				7.71	6.26	6.66	6.66	6.2 ^a	5.21	5.21	6.11	5.1	5.1	5.1	5.2 ^a	5.2 ^a					

8a. Experimental results (geometrical ZFE shape)

The outline limit of the ZFE is shown below. The geometrical shape of the ZFE is close to a conical one (for the instantaneous and time-averaged images) and to a ballistic one (for the RMS image). One can observe from the RMS image, that flow fluctuation (turbulence) is initiated at jet nozzle elevation. This is not easy to observe from the two other images, therefore one can erroneously claim that transition to turbulence occurs at higher elevations.

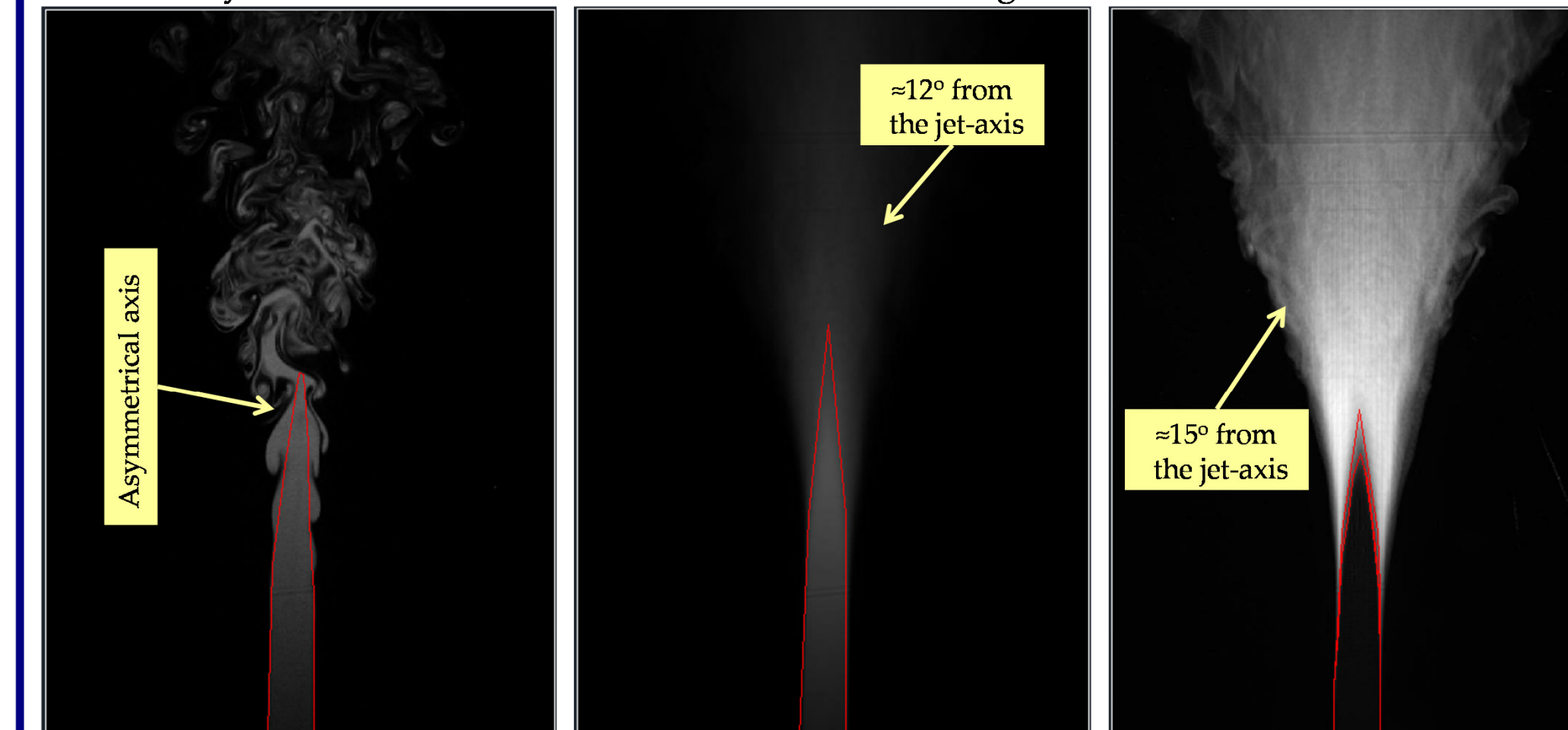


Figure 5: Outer limits (red color line) of the ZFE in an instantaneous (left), time-averaged (middle) and RMS (right) images (here, the inner line is shown as well). These images are taken from the 3rd experiment (D=1.5 cm). Scale is 1:2.

8b. Experimental results (ZFE length)

The mean and standard deviation distributions of the concentration along the jet-axis are shown below. The mean concentration should be constant within the ZFE but here is rising probably due to the fact that the initial concentration of R6G ($\approx 50 \mu\text{g/l}$) is high for the laser to pass through in a small area around the nozzle. Also, the distributions of the standard deviation do not show a successive decrease. This is because they are normalized with the maximum standard deviation observed within the ZFE which varied (measured 30 to 45% of the $C_{m,0}$).

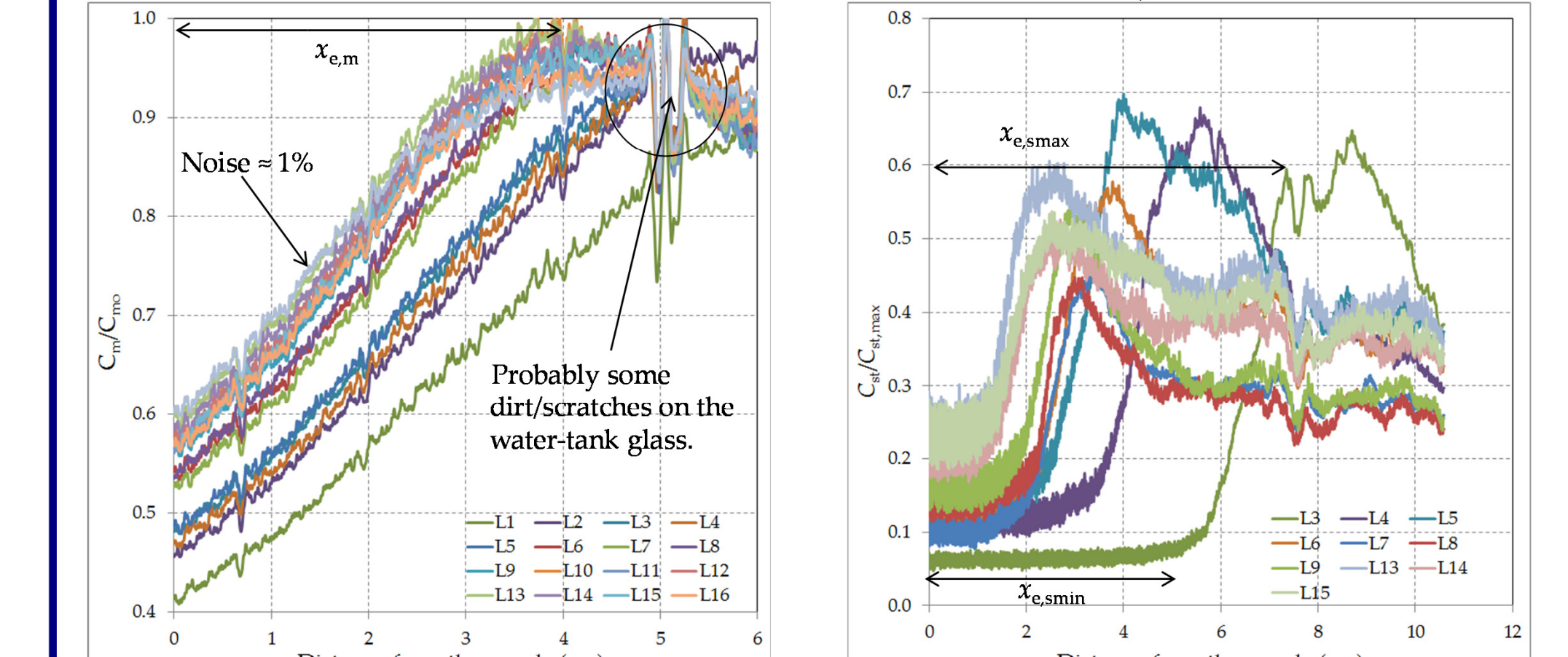


Figure 6: Mean C_m (left) and standard deviation C_m (right) distributions (normalized with their maximum values $C_{m,0}$ and $C_{m,0,max}$ respectively) along the jet-axis, from the 1st experiment (D=0.5 cm). For Li see section 7.

8c. Experimental results (graphs)

Graphs with all the measured ZFE lengths are presented below. It is observed that as Re increases, distance x_c decreases (with the exception of $x_{c,m}$ and $x_{c,smax}$ of the 3rd experiment). Also, the distances $x_{c,min}$ and $x_{c,smax}$ seem to be anti-symmetrical with respect to $x_{c,m}$.

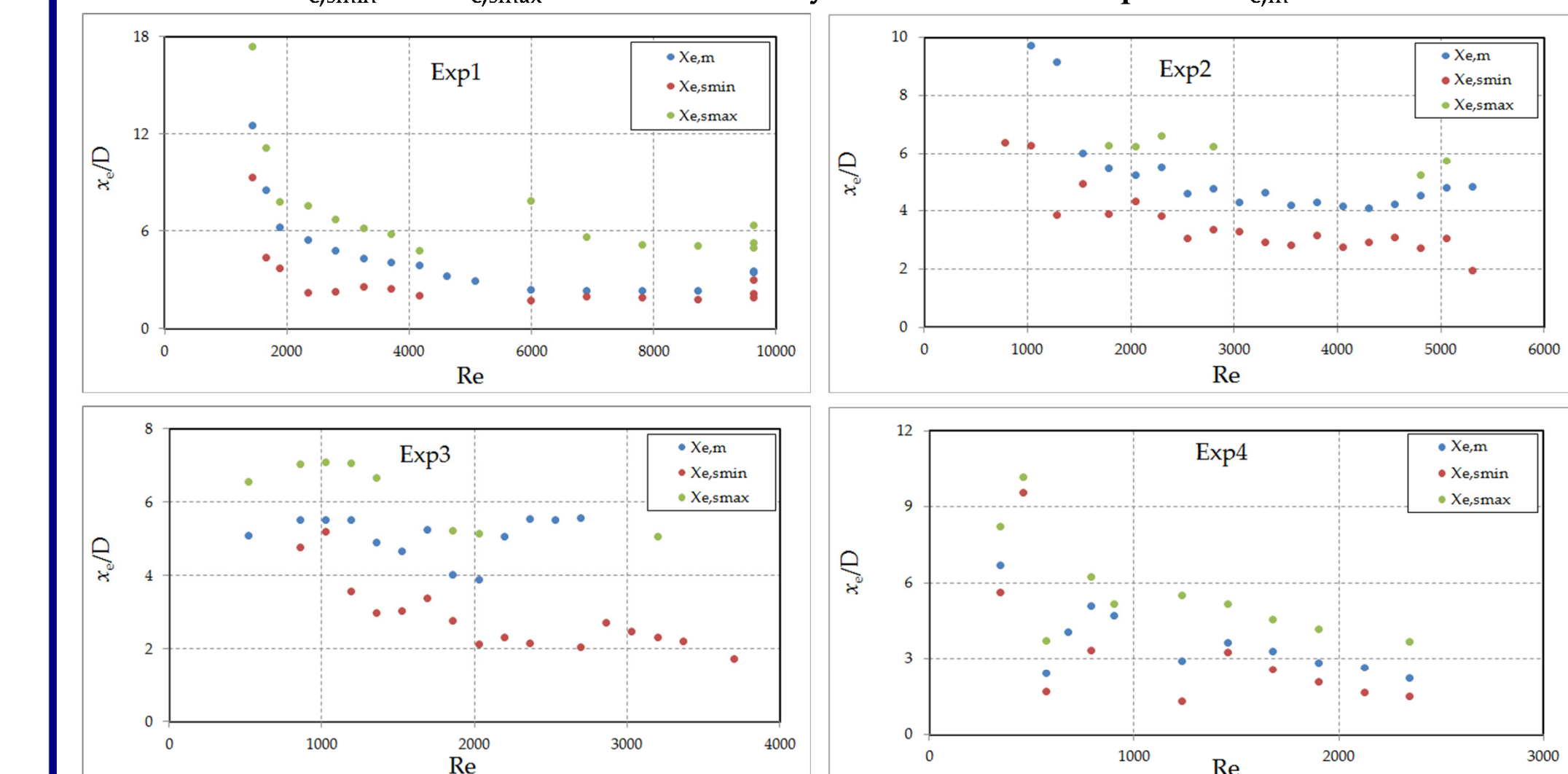


Figure 7: Measurements of the ZFE length versus Reynolds number taken from the experiments described above. Only values of green and yellow (symbolized with *) labels are presented.

9. Conclusions

The main conclusions of this work are as follows:

- The RMS image is much clearer than the time-averaged one, concerning the ZFE outer limit.
- The ZFE, defined through maximum RMS, seems to have a ballistic geometrical shape. Also, transition to turbulence seem to occur at the jet nozzle elevation.
- It is generally observed that as the Reynolds number increases, the ZFE length decreases.
- The present measurements of the ZFE are quite different than those proposed in earlier studies.

Acknowledgements

We acknowledge the free, collaborative and multilingual Internet encyclopedia Wikipedia (supported by the non-profit Wikimedia Foundation) for offering us some first scientific glances in several topics (from ISO notations to LIF techniques) and thus, saving us valuable time.

References

Abramovich GN, "The Theory of Turbulent Jets", MIT Press, ch. 5.1, p. 352-357, 1963.
 Albertson M L, Y B Dai, R A Jensen and H Rouse, Diffusion of Submerged Jets, J. Hydr. Div. ASCE, 94, p. 639-644, 1948.
 Chen J & C.P. Nikipoulos, On the Near Field Characteristics of Axisymmetric Turbulent Buoyant Jets in a Uniform Environment, Int. J. Heat Mass Transfer, Vol. 22, p. 245-255, 1979.
 Crow, S.C. and Champagne, F.H., Orderly structure in jet turbulence, J. Fluid Mech. Vol. 48, pp.547-596, 1971.
 Ferrier A., Fank D.R., and Roberts F.J.W., Application of optical techniques to the study of plumes in stratified fluids, Dynamics of Atmospheres and Oceans, Vol. 20, p. 155-183, 1993.
 Jirka G.H., Integral Model for Turbulent Buoyant Jets in Unbounded Stratified Flows, Part I: Single Round Jet, Environmental Fluid Mechanics, Vol. 4, p. 1-56, 2004.
 Henderson-Sellers B., The zone of flow establishment for plumes with significant buoyancy, Appl. Math. Modelling, Vol. 7, 1983.
 Hongwei W., Investigations of buoyant jet discharges using combined DPV and PLIF, PhD thesis in Civil and Structural Engineering, Nanjing Technological University, Singapore, 2000.
 Kovas S. & Li W. See, Reynolds number effects on the behavior of a non-buoyant round jet, Experiments in Fluids, Vol. 36, p. 881-882, 2003.
 Labus T. & F.P. Symons, Investigations of Free Jet With An Initially Uniform Velocity Profile, Louis Research Center, NASA Technical Note D-6783, 1972.
 Lee H.W. & G.H. Jirka, Vertical round buoyant jet in shallow water, Journal of the Hydraulics Division, Proc. ASCE, 107(HY12), p. 1651-1675, 1981.
 Pratte B.D. & W.D. Baines, Profiles of the Round Turbulent Jet in a Cross Flow, ASCE Journal of the Hydraulics Division, 92, HY6, 5556, 1, p. 53-64, 1967.
 Schatzmann M., The Integral Equations of Round Buoyant Jets in Stratified Flows, J. Appl. Math. Phys. (ZAMP), Vol. 29, N. 4, p. 608-630, 1978.
 Walker D.A., A Fluorescence Technique for Measurement of Concentration in Mixing Layers, J. Phys. Sci. Instrum., Vol. 20, p.217-224A, 1967.
 Xu G, Antonia RA, Effect of different initial conditions on a turbulent round free jet, Exp Fluids, Vol. 33, p. 677-683, 2002.